



Botrytis hypersensitive response inducing protein 1 triggers noncanonical PTI to induce plant cell death

Tanja Jeblick ¹, Thomas Leisen ¹, Christina E. Steidele ², Isabell Albert ³, Jonas Müller,¹
Sabrina Kaiser ¹, Florian Mahler ⁴, Frederik Sommer ⁵, Sandro Keller ^{4,6,7,8},
Ralph Hüchelhoven ², Matthias Hahn ¹ and David Scheuring ^{1,*}

- 1 Plant Pathology, University of Kaiserslautern, Kaiserslautern 67663, Germany
- 2 Phytopathology, TUM School of Life Sciences, Technical University of Munich, Freising 85354, Germany
- 3 Molecular Plant Physiology, FAU Erlangen, Erlangen 91058, Germany
- 4 Molecular Biophysics, University of Kaiserslautern, Kaiserslautern 67663, Germany
- 5 Molecular Biotechnology & Systems Biology, University of Kaiserslautern, Kaiserslautern 67663, Germany
- 6 Biophysics, Institute of Molecular Biosciences (IMB), NAWI Graz, University of Graz, Graz 8010, Austria
- 7 Field of Excellence BioHealth, University of Graz, Graz, Austria
- 8 BioTechMed-Graz, Graz, Austria

*Author for correspondence: scheurin@rhrk.uni-kl.de

C.E.S., R.H., S.K., M.H., and D.S. designed research. T.J., T.L., C.E.S., J.M., S.Ka., and D.S. conducted the majority of the experiments; F.S. performed MS-MS analysis; T.J. and F.M. carried out CD spectroscopy, I.A. conducted the calcein release assay. T.J., T.L., C.E.S., R.H., J.M., S.Ka., F.M., S.K., M.H., and D.S. analyzed data. D.S. created the figures and wrote the manuscript. All co-authors commented on the manuscript.

The author responsible for distribution of materials integral to the findings presented in this article in accordance with the policy described in the Instructions for Authors (<https://academic.oup.com/plphys/pages/general-instructions>) is David Scheuring (scheurin@rhrk.uni-kl.de).

Abstract

According to their lifestyle, plant pathogens are divided into biotrophic and necrotrophic organisms. Biotrophic pathogens exclusively nourish living host cells, whereas necrotrophic pathogens rapidly kill host cells and nourish cell walls and cell contents. To this end, the necrotrophic fungus *Botrytis cinerea* secretes large amounts of phytotoxic proteins and cell wall-degrading enzymes. However, the precise role of these proteins during infection is unknown. Here, we report on the identification and characterization of the previously unknown toxic protein hypersensitive response-inducing protein 1 (Hip1), which induces plant cell death. We found the adoption of a structurally conserved folded *Alternaria alternata* Alt a 1 protein structure to be a prerequisite for Hip1 to exert its necrosis-inducing activity in a host-specific manner. Localization and the induction of typical plant defense responses by Hip1 indicate recognition as a pathogen-associated molecular pattern at the plant plasma membrane. In contrast to other secreted toxic *Botrytis* proteins, the activity of Hip1 does not depend on the presence of the receptor-associated kinases BRI1-associated kinase 1 and suppressor of BIR1-1. Our results demonstrate that recognition of Hip1, even in the absence of obvious enzymatic or pore-forming activity, induces strong plant defense reactions eventually leading to plant cell death. *Botrytis hip1* overexpression strains generated by CRISPR/Cas9 displayed enhanced infection, indicating the virulence-promoting potential of Hip1. Taken together, Hip1 induces a noncanonical defense response which might be a common feature of structurally conserved fungal proteins from the Alt a 1 family.

Introduction

Successful plant pathogens need to overcome preformed and activated defense barriers of their hosts for infection. To overcome such barriers at the cuticle and the cell wall, small wounds or penetration sites are created by invasive pathogens, using either disruptive enzymes or physical force or both (Hématy et al., 2009). The necrotrophic fungus *Botrytis cinerea* (*Botrytis* hereafter), causal agent of the gray mold rot, has a wide host range of more than 1,000 species, and successful infection is usually characterized by rapid killing of plant cells and subsequent colonization of dead tissue (Williamson et al., 2007; Dean et al., 2012). During the infection process, large amounts of cell wall-degrading enzymes (CWDEs) and phytotoxic proteins are secreted, with many of them having unknown molecular functions.

Up to date, several cuticle- and CWDEs have been functionally characterized in *Botrytis*: For instance, CutA hydrolyses cutin (van Kan et al., 1997), pectin has been shown to be degraded by the endopolysaccharuronases PG1 and PG2 (Ten Have et al., 1998; Kars et al., 2005), the xylanases Xyn11A and Xyl1 and the xyloglucanase XYG1 (Brito et al., 2006; Noda et al., 2010; Zhu et al., 2017; Yang et al., 2018) target hemicellulose, while the endo- β -1,4-glucanase Cel5A degrades cellulose (Espino et al., 2005). Another class of proteins typically present in necrotrophic fungi are necrosis-inducing proteins (NIPs), consisting mainly of cerato-platanins, necrosis- and ethylene-inducing proteins (NEPs), and NEP-like proteins (NLPs). NLPs have been suggested to function by permeabilizing the plasma membrane (PM) to facilitate pathogen penetration (Schouten et al., 2008). Indeed, NLPs from plant-pathogenic oomycetes have been shown to bind to specific membrane lipids, conducting a pore-forming activity which eventually results in cell lysis (Lenarčič et al., 2017).

In addition to their original function, several secreted *Botrytis* proteins are recognized by the plant immune system as pathogen-associated molecular patterns (PAMPs), leading to PAMP-triggered immunity (PTI). Notably, enzymatically inactive mutant proteins are still capable of inducing cell death and often short conserved amino acid (aa) sequences could be identified as PAMP epitopes which are recognized by pattern recognition receptors (PRRs) at the plant PM (Boutrot and Zipfel, 2017). These surface receptors can occur in two main structural classes: receptor-like kinases (RLKs), and receptor-like proteins (RLPs) depending on the presence or absence of a cytoplasmic kinase domain, respectively. Inward signaling through both classes requires in the majority of described cases the interaction with one or several co-receptors (Boutrot and Zipfel, 2017). During the last decade, BRI1-associated kinase 1 (BAK1) and suppressor of BIR1-1 (SOBIR1) have been established as the most widespread co-receptors (Schellenberger et al., 2019). Strikingly, the necrotic activity of several secreted *Botrytis* proteins (e.g. Spl1, XYG1, and Xyl1), depends on the presence of BAK1 and SOBIR1 (Frías et al., 2011; Zhu et al., 2017; Yang et al., 2018). Although direct receptor binding has not yet been

demonstrated, many cell death-inducing PAMPs from *Botrytis* have been identified: among them are peptides from the xylanases Xyn11A (25 aa) and Xyl1 (26 aa), the cerato-platanin Spl1 (40 aa), the similar to IgE binding protein (IEB1, 35 aa), and nlp20, a 20 aa peptide which is found in most NLPs (Noda et al., 2010; Frías et al., 2011; Albert et al., 2015; Frías et al., 2016; Yang et al., 2018). Spl1 and IEB1 are both without known enzymatic activity, and it has been suggested that recognition as PAMP alone is sufficient for induction of necrosis. Although PTI is a relatively basal plant defense response, PAMPs can ultimately induce the hypersensitive response (HR), a strong local defense response involving programmed cell death (Thomma et al., 2011; Boutrot and Zipfel, 2017). Usually, the HR serves as a measure to protect plants from pathogen proliferation, but for necrotrophic pathogens this response has been shown to be beneficial (Govrin and Levine, 2000).

The generation of single knockouts mutants for the majority of phytotoxic *Botrytis* proteins showed only a mild reduction in virulence (Noda et al., 2010; Frías et al., 2011) or no effect on pathogenicity at all (Schouten et al., 2008; Cuesta Arenas et al., 2010; Frías et al., 2016; Zhu et al., 2017). Taken also into account that the majority of more than 200 proteins detected in the *Botrytis* secretome (Espino et al., 2010; Li et al., 2012; Frías et al., 2016; Zhu et al., 2017; Müller et al., 2018) are not well characterized yet, we hypothesized that additional, yet unknown, toxic proteins might exist. In this study, we report on a screen of the *Botrytis* secretome for additional phytotoxic proteins, which resulted in the identification and characterization of the previously unknown secreted HR-inducing protein 1 (Hip1). We show that the strong necrosis-inducing activity of Hip1 relies on almost the entire aa sequence of the protein and provide evidence that Hip1 has a fold similar to that of an allergen from *Alternaria alternata* (Alt a 1). Furthermore, we demonstrate that Hip1 induces early plant immune responses, suggesting recognition as a PAMP at the plant PM and induction of PTI. While *hip1* knockout did not alter the phenotype, overexpression of *hip1* in *Botrytis* led to a slightly, but significantly enhanced infection behavior, indicating a role in pathogenesis.

Results

Identification of a previously unknown toxic protein from *Botrytis*

To confirm that the toxicity of the *Botrytis* secretome produced during plant infection is mainly derived from proteins (Zhu et al., 2017), the secretome was subjected to heat treatment and digestion by proteinase K treatment prior to infiltration into *Nicotiana benthamiana* leaves (Supplemental Figure S1). After 8 h of incubation, we observed necrosis of the entire secretome-treated leaf area, whereas both heat and proteinase K treatments reduced the necrotic area to ~30% and ~20%, respectively. For the identification of as-yet uncharacterized phytotoxic proteins, the secretome was fractionated, using a combination of native ion exchange

chromatography and size exclusion chromatography. Toxicity of the resulting fractions was assessed by infiltration in *N. benthamiana* leaves. We defined toxicity as the ability to induce plant cell death. For simplicity, we refer to macroscopically visible dead areas of plant tissue as necrotic areas without specifying in which way cell death has been triggered. After infiltration, fractions that induced necrosis were subjected to mass spectrometry (MS)-based protein identification, and the candidate proteins were sorted by abundance and distribution in the individual fractions. Twenty-two *Botrytis* candidate genes encoding candidate toxic proteins (Supplemental Table S1) were cloned in a binary pGreen II vector, possessing a strong 35S promoter, a plant signal peptide (SP), and a hemagglutinin (HA) tag for expression control (Figure 1A). Using *Agrobacterium tumefaciens*-mediated transient expression in *N. benthamiana*, the presence of all proteins could be immunologically confirmed (Supplemental Figure S2) and necrosis-inducing activity was analyzed (Figure 1B).

Compared to the positive control (XYG1, Zhu et al., 2017), only candidate protein 22 (Bcin14g01200) showed similar necrosis-inducing activity. Previously, a homolog of candidate protein 22 has been described in the elm tree pathogen *Ophiostoma ulmi* as a phytoalexin-inducing protein (Yang et al., 1989; Taylor et al., 2008). Lower expression levels of candidate gene 22 induced spot-like necrotic lesions reminiscent of localized HR, and we thus named candidate gene 22 HR inducing protein (Hip1). Homologs of Hip1 are found in plant pathogenic and plant-associated ascomycetous fungi and seem to be restricted to the classes Leotiomyces (including *Botrytis*, *Sclerotinia*, *Monilinia*), Sordariomycetes (including *Colletotrichum*, *Fusarium* and *Podospira*), and Dothideomycetes. A Hip1 homolog, SsNE2, in *Sclerotinia sclerotiorum* has been recently described as a member of a group of necrosis-inducing effectors whose activity depends on the co-receptors BAK1 and SOBIR1 (Seifbarghi et al., 2020).

The majority of the Hip1 aa are needed to confer toxicity

Consideration of the Hip1 sequence revealed the presence of four conserved cysteine residues which were predicted to form two disulfide bridges (Figure 2A; Supplemental Table S2).

Since several secreted *Botrytis* proteins induce cell death in a PAMP-like manner, a search for a minimal (PAMP) cell death-inducing sequence was performed. For this, six truncated Hip1 versions, three lacking aa at the N-terminus and three lacking aa at the C-terminus were transiently expressed (Figure 2, A and B; Supplemental Figure S3). Only the truncation comprising aa 1–106 showed similar necrosis-inducing activity as full-length Hip1, while all other truncations were largely inactive (Figure 2C). Examination of *hip1* transcript levels in *Botrytis* during infection revealed an upregulation after 24 h in *N. benthamiana* with a peak at 72 h (Figure 2D), whereas expression in tomato (*Solanum*

lycopersicum) was generally weaker and declined at 72 h (Figure 2E).

A conserved adopted protein fold is crucial for toxicity

To confirm the results from transient expression, recombinant protein expression in *Escherichia coli* and subsequent purification were employed (Supplemental Figure S4). Starting at 0.5 μ M concentration, Hip1 showed necrosis-inducing activity 48 h post infiltration in *N. benthamiana* (Figure 3A).

Given that most of the Hip1 sequence is required for toxicity, 3D structure prediction was carried out. To this end, ColabFold, a software that combines MMseqs2 homology search with AlphaFold2 (Mirdita et al., 2022) was used, displaying a compact protein structure consisting of antiparallel β -sheets (Figure 3B). Cysteine residues at positions 18 and 25 are in close proximity on opposing β -sheets, and cysteine residues at positions 44 and 66 are located toward the inside of the structure model but also in close proximity (Figure 3B; cysteine residues highlighted in magenta). In addition to the use of ColabFold, structure prediction was also carried out by using the Phyre2 server, which performs modeling of sequences based on template sequences with known structures (Kelley et al., 2015). Based on X-ray crystallography of the *A. alternata* allergen Alt a 1 (Chruszcz et al., 2012), a similar β -barrel conformation was predicted for Hip1 with 80% confidence (Supplemental Figure S4). Notably, antiparallel β -sheets, forming a barrel-like structure are shared by MoHrip1 from *Magnaporthe oryzae* (Zhang et al., 2017) and Pevd1 from *Verticillium dahliae* (Zhang et al., 2019) (Supplemental Figure S4). Although Hip1 is not homologous to Alt a 1 and the two fungal effectors, it can also be considered as member of the family of Alt a 1 proteins. In order to investigate whether this putative fold is required for mediating toxicity, we challenged the folded state of Hip1 by different means. Dithiothreitol (DTT) was used to reduce disulfide bonds, heat treatment was employed for protein denaturation, and tryptic digest to hydrolyse peptide bonds. This resulted in a significant reduction of necrosis-inducing activity in case of DTT and heat treatment alone but around 50% activity remained. In contrast, the combination of DTT and heat treatment as well as tryptic digest almost entirely abolished toxicity (Figure 3C). To understand why toxicity was only partially decreased upon heat treatment, we tested Hip1 heat stability by circular dichroism (CD) spectroscopy. For this purpose, a temperature gradient ranging from 15°C to 95°C was applied, and the CD signal measured. As expected, this revealed a temperature-induced conformational change of Hip1 (Figure 3D, blue curves) which, however, was partly reversed upon cooling (Figure 3D, red curves). Although refolding was only partial, the observation that the midpoint of the temperature downscan fell close to that of the upscan indicates that part

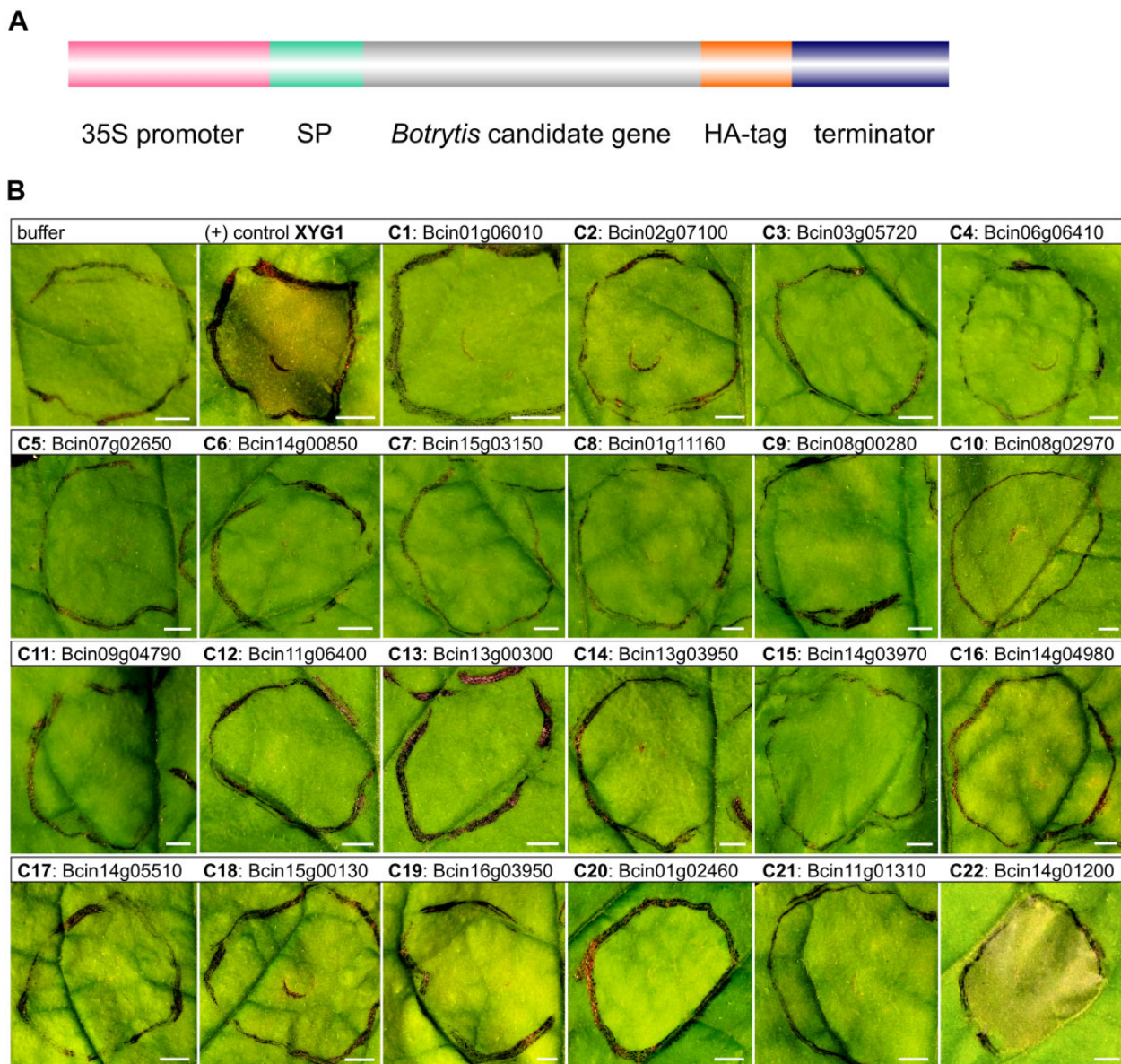


Figure 1 Screening for toxic *Botrytis* proteins. A, *Agrobacterium*-mediated transient expression using the CMV 35S promoter, a plant SP and an HA tag for detection. B, Symptoms on leaves of *N. benthamiana*. XYG1 (Zhu et al., 2017) was used as positive control and 22 genes encoding candidate proteins (C1–C22) were tested. Similar to XYG1, only candidate 22 showed substantial toxicity 3 days post infiltration, necrotizing the entire infiltrated leaf area. Scale bars = 4 mm.

of the protein regained its native conformation even after exposure to high temperature.

Delving deeper into the role of the active conformation, we replaced cysteine residues which were predicted to form disulfide bridges by site-directed mutagenesis. Therefore, we exchanged the cysteine at position 18 by serine to prevent bridge formation between the first predicted cysteine pair (between C18 and C25; Figure 2A). In addition, we replaced the cysteine residues at positions 18 and 44 together to prevent the formation of both disulfide bridges to disturb folding into Hip1's native conformation (Figure 2A). Upon transient expression, the necrotic activity of the single cysteine mutant (Hip1 C18S) was unaffected, whereas the necrotic activity of Hip1 C18S C44S was greatly reduced

(Figure 3E; Supplemental Figure S3). Together, this indicates a pivotal role of Hip1's native fold in conferring toxicity.

Hip1 induces plant defense responses in the apoplast

As recognition of PAMPs by PRRs usually takes place at the PM in plants (Boutrot and Zipfel, 2017), we aimed to confirm Hip1 localization by using live-cell imaging. A Hip1-green fluorescent protein (GFP) fusion displayed similar levels of necrosis-inducing activity (Supplemental Figure SSA) and, when transiently expressed, was found at cell borders of *N. benthamiana* leaf epidermal cells (Figure 4A and B). Co-localization studies, using the PM marker spRFP-TMD23 (Scheuring et al., 2012) showed Hip1-GFP in close proximity

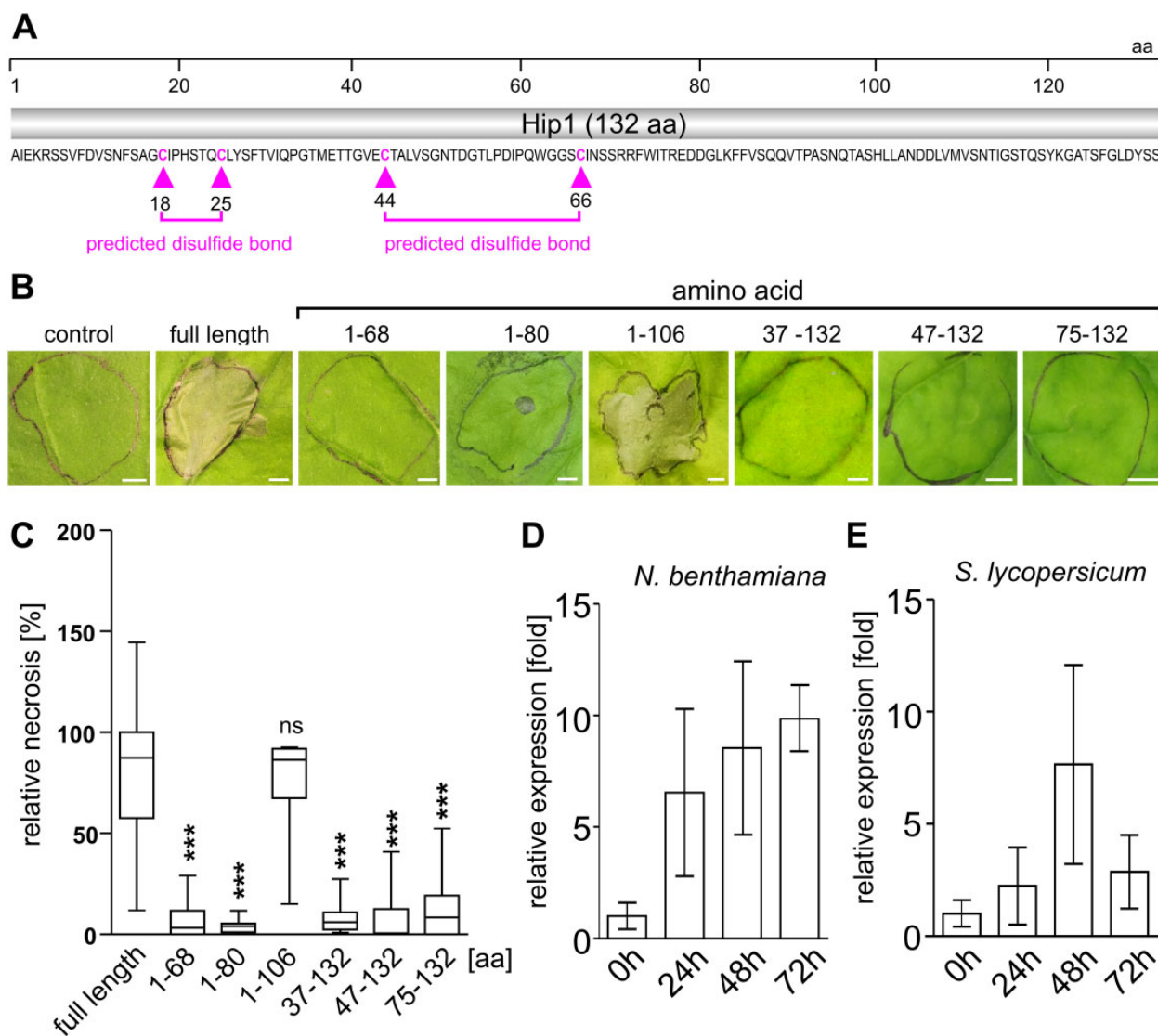


Figure 2 Toxicity of the Hip1 requires the majority of the underlying aa sequence. A, Aa sequence of Hip1 without SP. Conserved cysteine residues and predicted disulfide bridges are highlighted (arrow heads), the indicated position is based on the mature protein without SP. B, Different truncations were transiently expressed in *N. benthamiana*. Scale bars = 4 mm. C, All but the truncation comprising of aa 1–106 lost toxic activity. Significant differences compared with Hip1 (as a control) are shown (one-way analysis of variance (ANOVA) followed by Tukey's post hoc test; *** $P < 0.001$; $n > 8$). Box limits in the graphs represent 25th–75th percentile, the horizontal line the median and whiskers minimum to maximum values. D and E, RT–qPCR to assess *hip1* expression during *Botrytis* infection of *N. benthamiana* (D) and *S. lycopersicum* (E). Values are normalized to the 0-h control. Bar graph shows the mean of three biological replicates with the standard error.

to the PM (Figure 4C). Furthermore, the Hip1 signal was often localized between neighboring epidermal cells, indicating its position in the apoplast (Figure 4D). Collection and immunological analysis of the apoplastic fluid confirmed that Hip1-GFP was secreted into the cells' exterior (Figure 4E). To rule out a function inside of the cell, Hip1 was transiently expressed in *N. benthamiana* without SP. While there was never any sign of toxicity, expression levels of the SP-less Hip1 were very low. Only prolonged expression (120 h) yielded the detection of a weak signal which was slightly lower than that of the Hip1 with an SP (Supplemental Figures S5B and S5C).

To test whether Hip1 indeed functions as a PAMP, typical immune reactions indicative for a PTI were assessed. To this

end, reactive oxygen species (ROS) formation and ethylene accumulation were measured in *N. benthamiana* leaves upon Hip1 treatment. For both experimental setups, the classical bacterial flagellin-derived PAMP-elicitor flg22 (Felix et al., 1999) was used as positive control. Indeed, Hip1 treatment led to the accumulation of ROS (Figure 4F) and ethylene (Figure 4G). Furthermore, accumulation of the phytohormone salicylic acid (SA) was determined upon Hip1 infiltration. Expression of the SA marker gene PR1 increased more than 100-fold already after 12 h (Figure 4H) and SA accumulated to levels that are 30-fold higher than in noninfiltrated leaves (Figure 4I). Notably, while plant wounding during infiltration contributes to

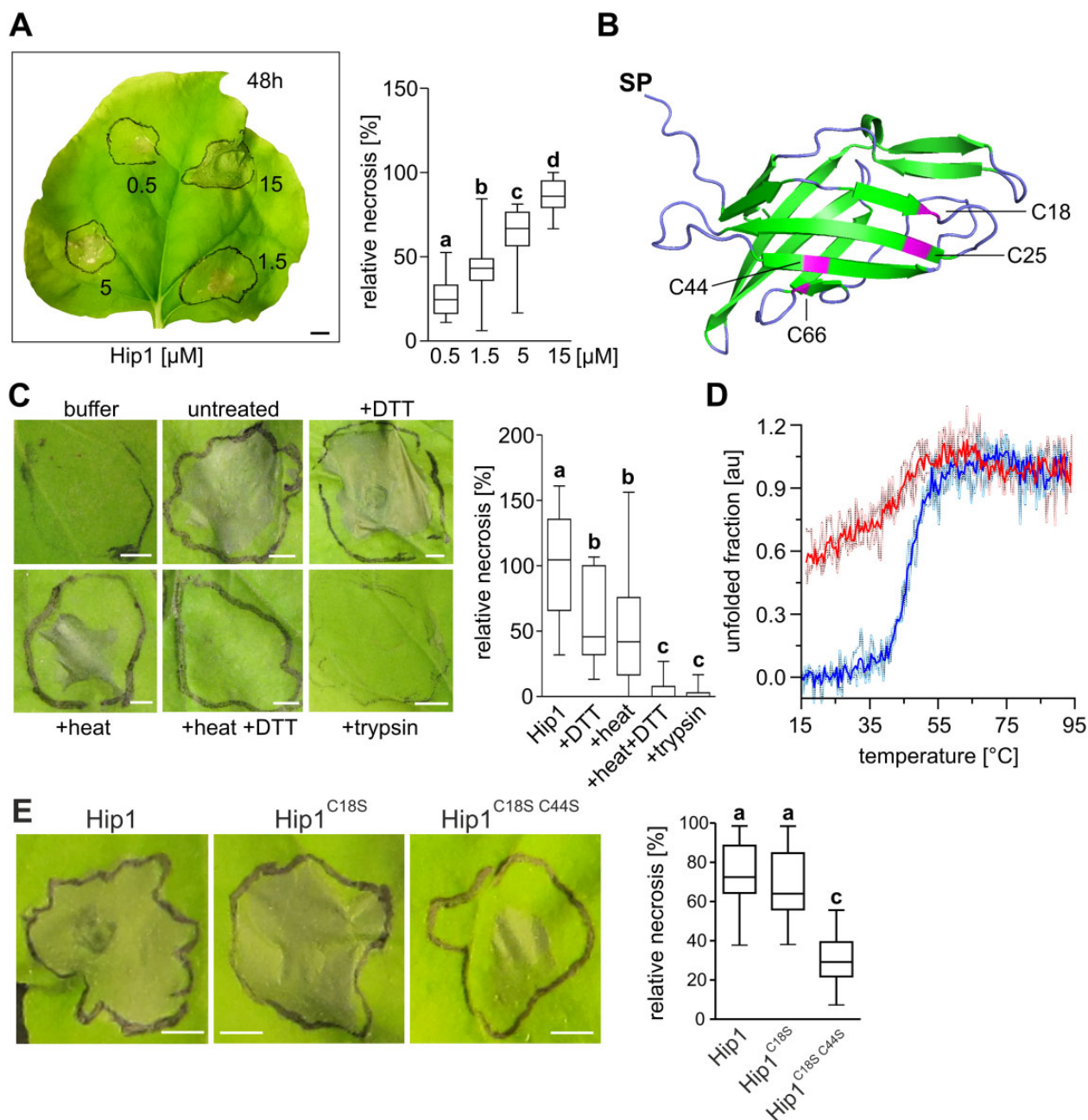


Figure 3 Evidences of the role of tertiary structure in Hip1 activity. **A**, Necrotic activity of different Hip1 protein concentrations was analyzed by protein infiltration into *N. benthamiana*. The image was digitally extracted for better visibility of necrotic areas. Different letters indicate significant differences between the individual bars (one-way ANOVA followed by Dunnett's multiple comparison post hoc test; b: $P < 0.01$; c: $P < 0.001$, d: $P < 0.001$; $n = 20$). **B**, AlphaFold 3D protein structure prediction using ColabFold. The tool DISULFIND (<http://disulfnd.disi.unitn.it/>) predicted disulfide bonds between C18 and C25 as well as between C44 and C66. **C**, Effects of different treatments of Hip1 protein on its phytotoxic activity. Different letters indicate significant differences according to one-way ANOVA followed by Dunnett's multiple comparison post hoc test ($P < 0.01$; $n > 12$). **D**, Thermal unfolding (blue) and refolding (red) of Hip1 monitored by CD spectroscopy. **E**, Necrotic activity upon transient expression of Hip1 point mutations, replacing the cysteine's on positions 18 and 44 by serine. Different letters indicate significant differences according to one-way ANOVA followed by Dunnett's multiple comparison post hoc test ($P < 0.01$; $n > 18$). Box limits in the graphs represent 25th–75th percentile, the horizontal line the median and whiskers minimum to maximum values. Scale bars = 4 mm (A, C, and E).

increased SA levels, the accumulation of jasmonic acid is highly specific to Hip1 infiltration and the increase more pronounced (Figure 4). Taken together, these results strongly suggest a PAMP-activity of Hip1 which in turn induces plant PTI.

Hip1 toxicity is host specific and independent of cytolytic activity and of the receptors BAK1 and SOBIR1

Notably, Hip1 showed differential activity depending on the tested host plants. Despite the wide host range of *Botrytis*,

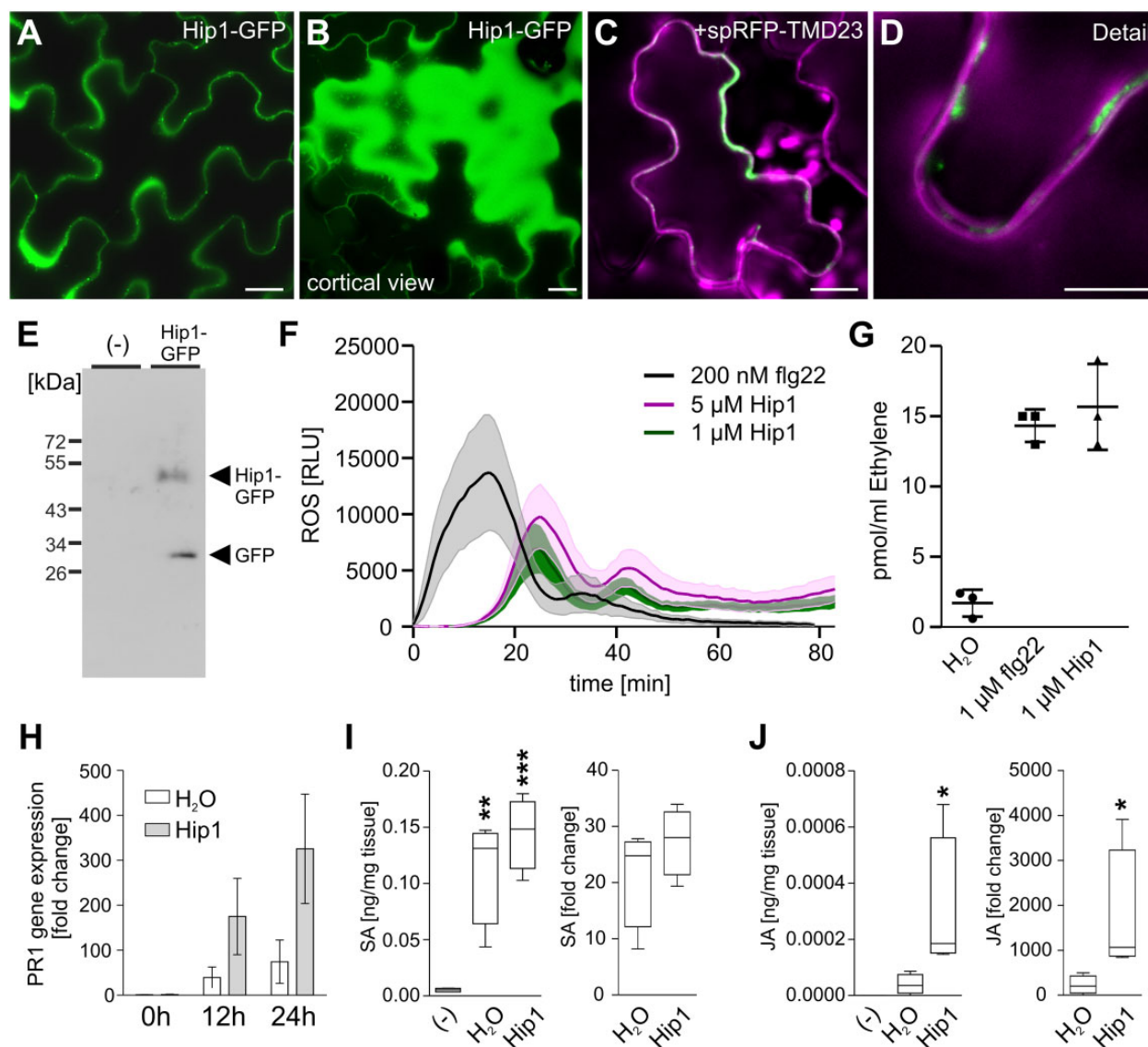


Figure 4 Hip1 is secreted and recognized as PAMP. A, Hip1-GFP highlights the borders of epidermal *N. benthamiana* cells when transiently expressed. B, The periclinal view of transformed cells indicate secretion of Hip1-GFP into the apoplast. C and D, Co-expression of Hip1-GFP with the PM marker spRFP-TMD23. Scale bars: 15 μm (A–D). E, Detection of Hip1-GFP within the apoplastic fluid of transiently transformed *N. benthamiana*. F, ROS measurement of different Hip1 protein concentrations and the prototypical PAMP flg22 as control. $n = 4$ leaf discs; experiment was repeated three times with similar results. Shaded areas represent standard error of the mean. G, Ethylene accumulation 3 h after treatment with Hip1 and flg22 as control for PAMP activity. Each data point represents three leaf discs measured in one vial. The experiment was repeated three times with similar results. Error bars represent standard deviation. H, RT-qPCR to assess PR1 gene expression upon infiltration with 15-μM Hip1 protein. H₂O was infiltrated as control. Bar graph shows the mean of three biological replicates with the standard error. Measurement of SA content 12 h after H₂O (control) and 15-μM Hip1 infiltration. J, Jasmonic acid (JA) measurement upon H₂O and Hip1 infiltration (12 h). For (I) and (J), the fold change was calculated in respect to the noninfiltrated samples (-). One-way ANOVA followed by Dunnett's multiple comparison post hoc test against noninfiltrated samples was carried out for absolute hormone levels and a Mann-Whitney t test to compare fold changes between H₂O (control) and Hip1 infiltration; * $P < 0.05$; ** $P < 0.01$; *** $P < 0.001$. Experiments in (I) and (J) were carried out as quadruplicate. Scale bars = 4 mm.

we observed remarkably different toxicity even within the same plant family (Solanaceae). While the infiltrated area become entirely necrotic within 72 h in *N. benthamiana* (Figure 5A), necrosis in *Phaseolus vulgaris* was slightly reduced (Figure 5B) and in *Solanum lycopersicum* considerably reduced (Figure 5C). In *Arabidopsis* (*Arabidopsis thaliana*)

leaves, no necrosis was induced and, in line with this, no significant ethylene accumulation was observed (Figure 5D).

Based on a similar fold of the structurally related PevD1 and an NLP from *Pythium aphanidermatum* (Ottmann et al., 2009), it was speculated that members of the Alt a 1 family might also possess cytolytic activity as it has

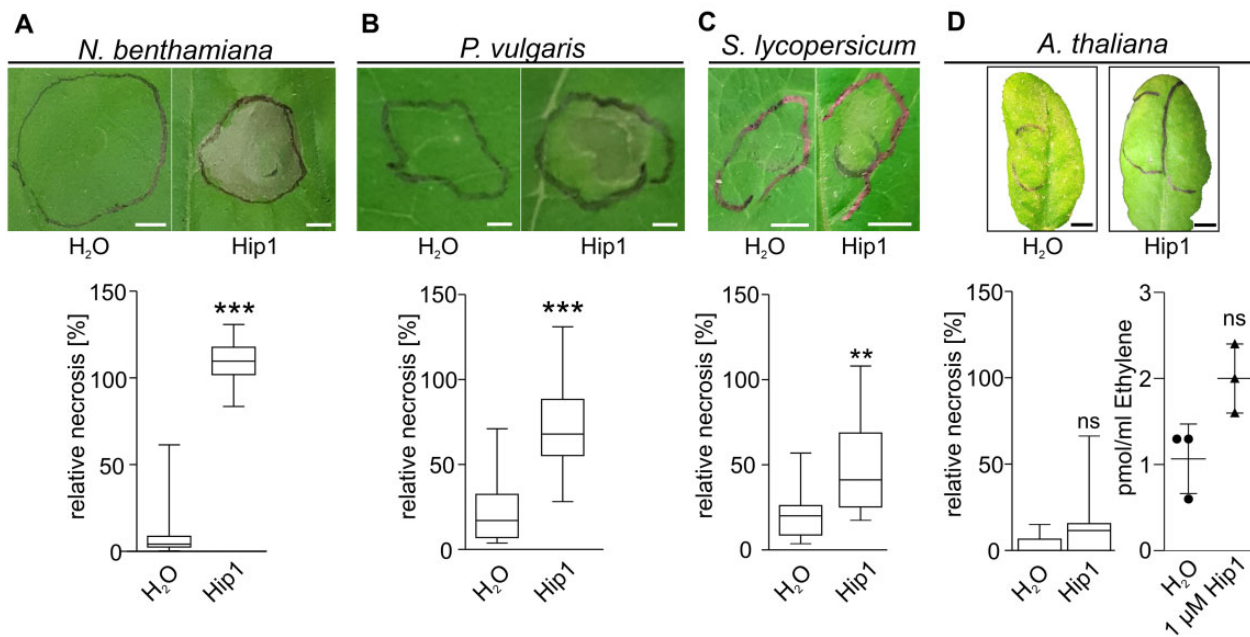


Figure 5 Hip1 displays differential toxicity dependent on the host plant. Hip1 protein (15 μM) was infiltrated into leaves and necrosis formation documented after 72 h. A, Toxicity in *N. benthamiana*; $n = 19$ infiltrations in nine plants, (B) toxicity in *P. vulgaris*; $n = 25$ infiltrations in 12 different plants, (C) toxicity in *S. lycopersicum*; $n = 26$ infiltrations in 13 plants, and (D) toxicity in *A. thaliana*, $n = 14$ infiltrations in 12 different plants. Images were digitally extracted for comparison. Box limits in the graphs represent 25th–75th percentile, the horizontal line the median and whiskers minimum to maximum values. Ethylene accumulation was measured 3 h after treatment with Hip1. Each data point represents three leaf discs measured in one vial. The experiment was repeated three times with similar results. Error bars represent standard deviation. For all panels, significant differences compared with the H₂O treatment are shown (Mann–Whitney test; ns = not significant; ** $P < 0.01$; *** $P < 0.001$).

been shown for NLPs. Due to the structural similarity of Hip1 and Alt a 1, and the requirements of most aa for toxic activity, we evaluated the possibility of a pore-forming function of Hip1. To this end, PM vesicles from *N. benthamiana* were loaded with the fluorophore calcein and its release was investigated in the presence of Hip1. Intact vesicles do not show fluorescence emission due to quenching while disintegration of membranes due to cytolytic activity results in calcein release and fluorescent light emission (Figure 6A). In contrast to NLP as positive control, the addition of Hip1 or H₂O did not lead to any release of calcein (Figure 6B). Since the receptor-associated kinases BAK1 and SOBIR1 participate in the majority of described receptor–ligand-induced PTI reactions (Schellenberger et al., 2019), we also tested Hip1 activity in the absence of both co-receptors. Therefore, we infiltrated *N. benthamiana* knockout lines for SOBIR1/SOBIR1-like (Huang et al., 2021) as well as BAK1 and SOBIR1 knockdown lines based on virus-induced gene silencing (VIGS) (Figure 6, C and E).

BAK1 silenced plants showed stunted growth and epinasty (as reported previously) and BAK1 and SOBIR1 expression was downregulated to 41% and 46% of wild-type levels, respectively (Supplemental Figure S6). However, quantification of necrosis development did neither show differences in the CRISPR knockout lines *sobir1/sobir1-like* nor in VIGS-silenced plants when compared to the wild type (Figures 6D and 6F).

Hip1 overexpression indicates function as virulence determinant

Next, we aimed to examine if Hip1 contributes to general virulence of *Botrytis*. Due to the high redundancy of phytotoxic compounds secreted by *Botrytis*, single knockout mutants often remain phenotypically inconspicuous (Leisen et al., 2022). To overcome this, we used CRISPR/Cas9 mutagenesis (Leisen et al., 2020) to establish overexpressor strains and test their infection behavior. For insertion of an additional copy of *hip1* driven by the H2B promoter into the *Botrytis* B05.10 wild-type strain, a nonessential region of chromosome 3 between two highly expressed genes (*sp11* and *xyn11a*) was chosen (Figure 7, A and B). Using reverse transcription–quantitative PCR (RT–qPCR), we could show that *hip1* expression in the transformants was moderately increased in vivo and in vitro (Supplemental Figure S7). For precise comparison, wild-type and overexpressor strains were inoculated on the same leaflet/leaf, and the lesion formation relative to wild-type was calculated (relative infection, Supplemental Figure S8). Both overexpressor strains displayed slightly but significantly increased infection on *P. vulgaris* (Figure 7D). This increase was more pronounced 72-h post inoculation, a time point where also overexpressor strain #4 showed increased infection of tomato (Figure 7C).

To confirm that increased Hip1 levels indeed contribute to the fitness of *Botrytis* (i.e. virulence), we analyzed early stages of infection microscopically. On detached *P. vulgaris* leaves, hyphal growth of overexpressor strains and wild-type

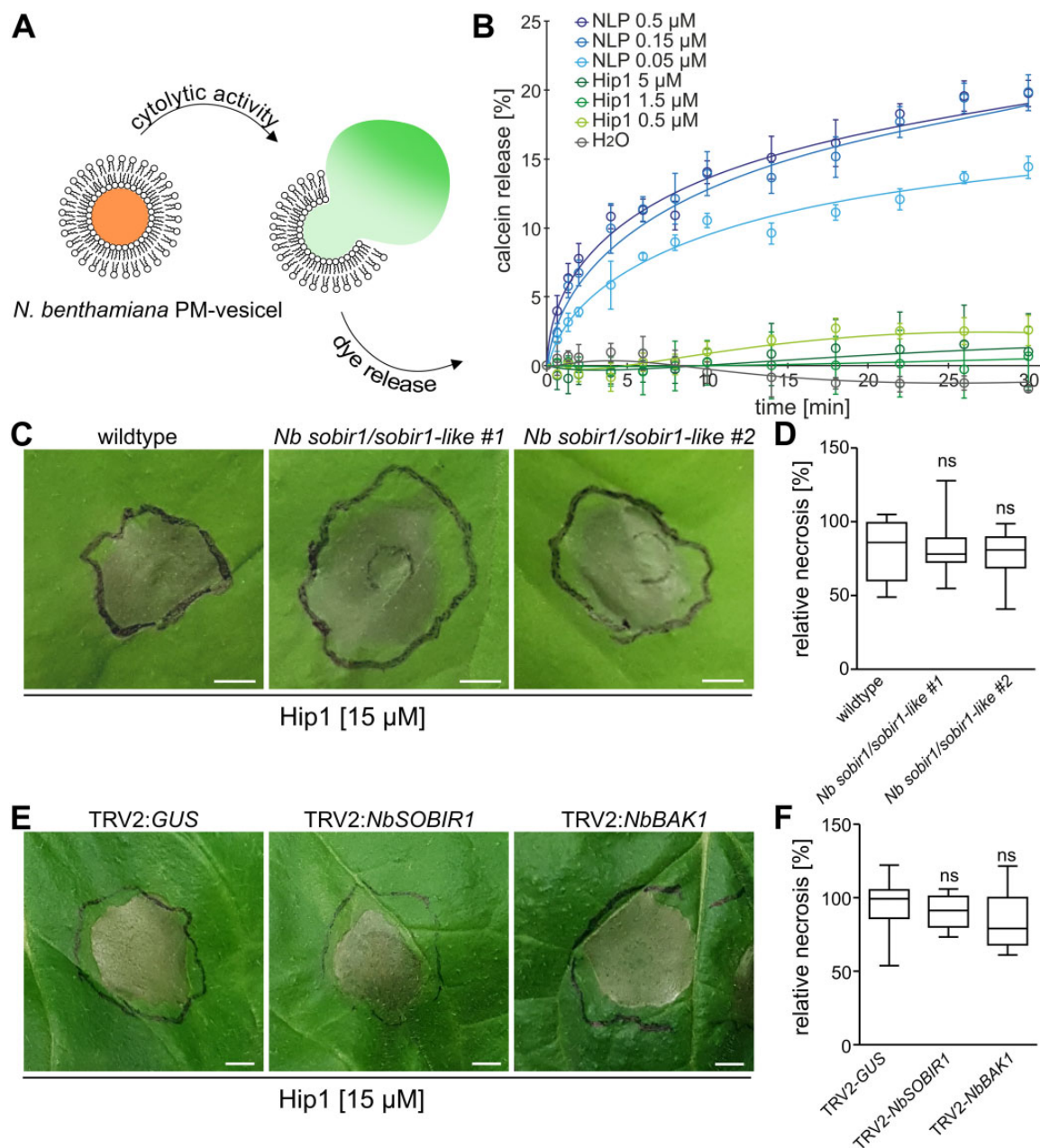


Figure 6 Hip1 toxicity is independent of cytolysis and does not rely on the receptor-associated kinases BAK1 and SOBIR1. **A**, Potential cytolytic activity of Hip1 was assessed by using a vesicle-based assay. Intact fluorophore calcein-loaded *N. benthamiana* PM vesicles do not show fluorescence emission due to quenching. Disintegration of membranes due to cytolysis by NLP results in calcein release and fluorescent light emission. **B**, Addition of Hip1 or H₂O did not lead to a release of calcein. Values represent means of $n = 3$ measurements \pm standard deviation. Similar results were obtained in three independent experiments. **C**, Two different *N. benthamiana* *sobir1* knockout lines were infiltrated with 15 μ M Hip1 protein and necrosis formation assessed after 48 h. Scale bars = 4 mm. **D**, Quantification of necrosis formation, $n > 12$. Significant differences compared with the wild-type are shown (one-way ANOVA followed by Dunnett's multiple comparison post hoc test; ns = not significant; $P \geq 0.05$). **E**, Results of infiltration of Hip1 into *N. benthamiana* after virus-induced gene silencing of β -glucuronidase (*GUS*) (control), *SOBIR1* and *BAK1* using TRV. Scale bars = 4 mm. **F**, Quantification of necrosis formation, $n > 6$. Significant differences compared with the control (TRV:*GUS*) are shown (one-way ANOVA followed by Dunnett's multiple comparison post hoc test; ns = not significant; $P \geq 0.05$). Box limits in the graphs represent 25th–75th percentile, the horizontal line the median and whiskers minimum to maximum values.

were measured 20 h post inoculation (Figure 7E). While mycelium growth in vitro and sporulation was comparable (Supplemental Figure S7), the overexpressor strains occupied a significantly larger space on the leaf, indicating a beneficial role of increased Hip1 levels on infection (Figure 7F).

Discussion

The infection success of *Botrytis* has been reported to depend on the secretion of a complex mixture of CWDEs, NIPs, phytotoxic metabolites, small ribonucleic acids, and

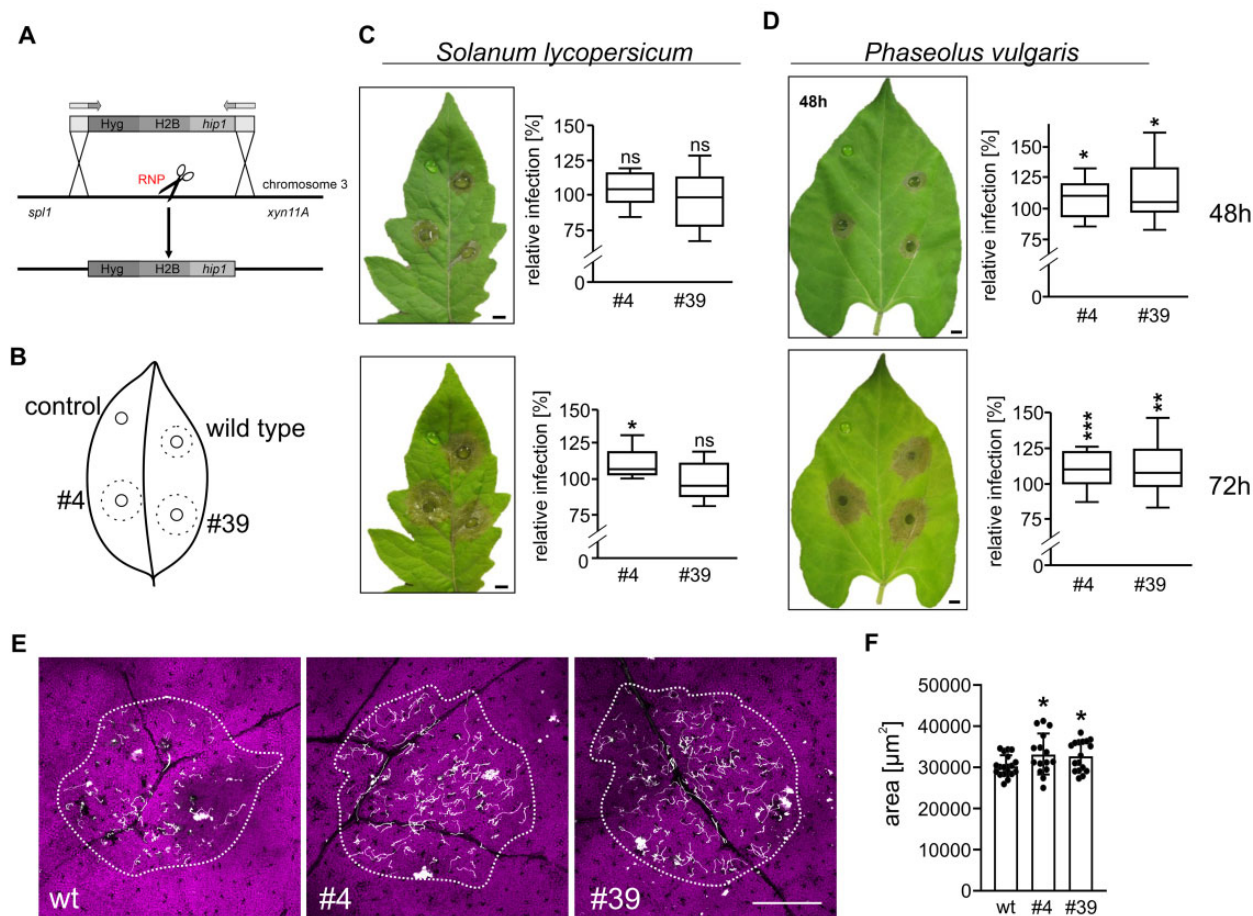


Figure 7 Hip1 overexpression in *Botrytis* facilitates infection. A, CRISPR/Cas9 as a ribonucleoprotein (RNP) was employed to insert *hip1* under control of the H2B promoter on chromosome 3 between *spl1* and *xyn11A* genes. B, Inoculation of two different overexpressor strains in comparison to *Botrytis* wild-type and a buffer control. C, Infection behavior on detached tomato (*S. lycopersicum*) leaflets 48 h and 72 h after inoculation. $n > 10$. D, Infection of bean leaves (*P. vulgaris*) 48 h and 72 h post inoculation. $n > 15$. Scale bars = 4 mm (C and D). Images were digitally extracted for better visibility of infections. For (C) and (D), wild-type and overexpressor strains were inoculated on the same leaflet/leaf and the relative secondary lesion was calculated in respect to the wild-type which was set to 100% (relative infection). Significant differences compared with a hypothetical value of 100% (wild-type) are shown (one-sample *t* test; ns = not significant; * $P < 0.05$; ** $P < 0.01$; *** $P < 0.001$). Box limits in the graphs represent 25th–75th percentile, the horizontal line the median and whiskers minimum to maximum values. E, Hyphal growth on detached *P. vulgaris* leaves (20 hpi). Fungal hyphae were stained with calcofluor white; scale bar: 500 μm . F, Quantification of hyphal occupancy. Data of three individual experiments are displayed with the standard error ($n > 15$). Significant differences compared with the wild-type are shown (one-way ANOVA and Dunnett's post hoc test; * $P < 0.05$).

various organic acids (van Kan, 2006; Weiberg et al., 2013; Müller et al., 2018; Veloso and van Kan, 2018). Impairment of the proteinaceous portion of the secretome largely abolishes necrosis-inducing activity (Supplemental Figure S1; Zhu et al., 2017). This suggests that it is mainly proteins that are contributing to toxicity and questions the major role of other metabolites and compounds. By fractionating the *on planta* secretome and analyzing candidate proteins for their phytotoxicity by agroinfiltration, we here identified a previously unknown phytotoxic protein—Hip1 (Fig 1). Although several toxic proteins have been identified over the last two decades in *Botrytis*, for many of them it remains elusive how they induce host cell death. Interestingly, the secreted proteins Xyn11A (Noda et al., 2010) and IEB1 (Frías et al., 2016) are able to trigger necrosis induction independently of their enzymatic function. For both, short peptides (25 aa and 35

aa) have been shown to be sufficient to induce PTI and this in turn seems to be linked to their toxic activity. The observed partial inactivation of Hip1 by heat or DTT (Figure 3), can be explained by partial refolding upon cooling and limited access of cysteine residues within the folded protein. Irreversible unfolding, however, largely abolished the necrosis-inducing toxicity of Hip1, indicating a crucial role of the tertiary structure of the protein for activity. Heat treatments also do not abolish the activity of several other NIPs, like endopolygalacturonase (PG) 3 (Zhang et al., 2014b) and SsCut from *S. sclerotiorum* (Zhang et al., 2014a), and in the case of latter the entire N-terminal half of the protein has been demonstrated to be dispensable for defense induction. Conversely, the tertiary structures of XYG1 (Zhu et al., 2017) and Spl1 (Frías et al., 2014; Frías et al., 2016) are crucial for necrosis and PTI induction, as heat treatment indeed

abolishes their function. In the case of Hip1, no short peptide conferring toxicity could be identified (Figure 2 and Supplemental Figure S4) and mutation of two cysteine residues, potentially interfering with the native conformation, abolished the toxic activity almost entirely (Figure 3E). If Hip1 is recognized by a PAMP receptor (PRR), this could indicate that recognition depends on an epitope that is formed only upon proper protein folding. Localization at the PM, detection within the apoplastic fluid, and the induction of typical immune responses suggest that Hip1 toxicity indeed relies on its recognition as PAMP (Figure 4). We noticed that in comparison to the flg22-induced ROS burst, the ROS amplitude induced by Hip1 was lower and the response slightly delayed (Figure 4F). This might be explained by the difference in size of the two elicitors as they must diffuse through the cell wall prior to receptor binding. Naturally, a small peptide-like flg22 diffuses faster than an entire 15-kDa protein (Hip1) which could impact ROS kinetics. Just very recently, the bacterial elicitor translation initiation factor (IF1) has been suggested to need tertiary fold features for receptor activation, inducing a later and weaker ROS burst than flg22 (Fan et al., 2022).

Notably, 3D protein structure prediction strongly suggests that Hip1 belongs to a fungal class of structurally, but not sequence-related proteins, termed the Alt a 1 family (Pfam family PF16541; Chruszcz et al., 2012). For several members of this family, namely MoHrip1, Pevd1, and SsNE2 defense and necrosis-inducing activity have been reported (Wang et al., 2012; Zhang et al., 2017; Zhang et al., 2019; Seifbarghi et al., 2020) but their biological function is still unclear.

Although PTI is usually associated with basal immunity, some PAMP-like proteins have been shown to induce cell death during the plant HR, typically a feature of effector-triggered immunity (ETI) (Jones and Dangl, 2006). For instance, CBEL, a protein from *Phytophthora parasitica* var *nicotianae*, is recognized as PAMP and induces HR-like lesions and defense responses (Gaulin et al., 2002; Khatib et al., 2004). Certain harpins from *Pseudomonas syringae* likewise represent PAMPs that seem to interfere with host membrane integrity (He et al., 1993; Engelhardt et al., 2009). In this context, it seems plausible that the necrosis-inducing activity of Hip1 results from HR-associated cell death and not from a toxic effect. Indeed, plant cell death has contrasting roles in defense against necrotrophs and biotrophs. While the HR in response to biotrophic pathogens is an indicator of resistance, it is beneficial for necrotrophic pathogens (Mengiste, 2012; Pitsili et al., 2020). Enhancing plant cell death has been demonstrated to increase susceptibility against *Botrytis* and might even be considered as hallmark of successful infection by necrotrophs (Govrin and Levine, 2000; Veronese et al., 2004; Govrin et al., 2006). Several *Botrytis* CWDEs and NLPs possess PAMP activity in addition to their enzymatic or pore-forming function. Even PAMP activity of proteins without enzymatic function (e.g. IEB1 and Spl1) has been shown to be sufficient to induce necrosis concomitant with plant defense reactions.

Interestingly, both Hip1-induced ethylene accumulation and toxicity were almost entirely absent in *Arabidopsis* (Figure 5). This indicates that induction of plant defense and toxic activity in case of Hip1 are tightly linked and not separable as it was shown for other secreted toxic proteins, for example XYG1 (Zhu et al., 2017). For one of the Alt a 1 family members, PevD1, it has been shown that the β -barrel core has a similar fold in comparison to an NLP from *Pythium aphanidermatum* (Ottmann et al., 2009; Zhou et al., 2017). Thus, it was speculated that PevD1-like proteins, may have a similar (pore-forming) function as NLPs during infection (Zhou et al., 2017). Despite the predicted high structural similarity of Hip1 and Alt a1, no cytolytic activity was observed (Figure 6). This questions a general lytic function of the Alt a 1 family and although it cannot be excluded that Hip1 has another, yet unknown, function, it seems possible that its main purpose is the (over) activation of plant immunity to accelerate plant cell death. This beneficial manipulation of plant defense has been described for host-specific necrotrophic effectors but their activity is restricted to host plants with an appropriate genotype (Oliver and Solomon, 2010). Since Hip1 homologs are widespread in plant pathogenic and plant-associated ascomycetous fungi (Supplemental Table S2), it seems possible that their toxicity is mediated solely via PTI manipulation.

In contrast to several other phytotoxic proteins (Frías et al., 2011; Kettles et al., 2017; Zhu et al., 2017; Seifbarghi et al., 2020), the present study shows that Hip1 toxicity is not dependent on the receptor-associated kinases BAK1 and SOBIR1 (Figure 6). This suggests recognition by RLKs and not RLPs which seems to be unique for a secreted toxic *Botrytis* protein. Independency from BAK1 could further indicate that a nonleucine-rich repeat (LRR)-RLK may be involved since LRR-RLKs usually act BAK1 dependently. Interestingly, the cell death-inducing activity of a PAMP, VmE02, from the necrotrophic fungus *Valsa mali*, has been shown to depend on the presence of a host-specific RLP at the PM of *N. benthamiana* (Nie et al., 2019; Nie et al., 2020). It is conceivable that the differential Hip1 toxicity is relying on binding of an, as yet unknown, BAK1-independent RLK at the cell surface. Furthermore, differential toxicity even within the same plant family (Solanaceae) indicates a highly variable distribution of PRRs in different plants or different binding affinities of homologous receptors for the same ligand. For Brassicaceae, it has been shown that recognition of PAMPs derived from fungal endopolygalacturonases depends on polymorphic RLPs with distinct specificities (Zhang et al., 2021). So it seems possible that receptors from the RLK class recognize structurally conserved protein folds from proteins of the Alt a 1 family.

Several CWDEs and NLPs of *Botrytis* possess PAMP activity in addition to their enzymatic or pore-forming function. Thus, it is not surprising that knockout of individual proteins from the toxic cocktail of secreted proteins rarely results in obviously different phenotypes (Leisen et al., 2022). Therefore, knockout of single proteins might individually

not alter the phenotype but together could be causal for the broad host spectrum of *Botrytis*. On the other hand, *hip1* overexpression led to enhanced infection, showing its potential to support virulence. Taken together, several aspects of Hip1 function are not in line with canonical PTI: instead of a short peptide, Hip1 needs almost the entire aa sequence and correct folding to confer toxicity (1), its activity is independent of the co-receptors BAK1 and SOBIR1 (2), and the amplitude of necrosis induction is strongly host dependent (3). In conclusion, this noncanonical PTI adds another layer of complexity within the *Botrytis* infection strategy. The described Hip1 function could represent a structurally conserved mechanism of fungal pathogens to overwhelm a broad spectrum of host plants.

Materials and methods

Plant materials and growth conditions

For leaf infiltration and transient expression, *N. benthamiana* was grown for 4–6 weeks on soil in long-day conditions (14-h light/10-h dark) at 23°C. For infiltration of Hip1 protein and infection tests, *P. vulgaris* (genotype N9059), *N. benthamiana*, and tomato (*S. lycopersicum*) ‘Marmande’ were grown under similar conditions, while Arabidopsis (*A. thaliana*) ecotype Col-0 was grown under long-day regime (16-h light/8-h dark) for 4 weeks at 22°C.

Cultivation of *Botrytis* and infection tests

Botrytis cinerea B05.10 was used as wild-type strain for infection tests, growth tests, secretome production, and as genetic background for *hip1* overexpression. Cultivation of *Botrytis* was performed as described previously (Müller et al., 2018). Infection tests were carried out using 1×10^5 spores mL^{-1} for tomato and *P. vulgaris* and 1×10^6 spores mL^{-1} for Arabidopsis. Due to the hydrophilic surface of *N. benthamiana* leaves inoculation using spore suspensions did not work well. Therefore, before infection, 10 μL of conidia (1×10^5 spores in liquid Gamborg medium with 25 mM glucose) were inoculated onto agar discs (5 mm \varnothing , 2 mm thickness; containing Gamborg medium with 25-mM glucose) and incubated overnight. The discs were placed with the germinated spores oriented downwards onto the leaves, and an additional 10 μL of Gamborg was added on top of the plaques. In general, lesions were photographed after 24 h, 48 h, and 72 h, and inoculation droplet size and lesion size were quantified (area) using the freehand tool in ImageJ. Lesion minus droplet size results in secondary lesion size which we used to calculate the ratio between the overexpression strain and wild-type. The relative infection was calculated based on B05.10 wild-type set to 100% and the *hip1* overexpressor strains on the same leaf.

Recombinant plasmid construction

Coding sequences were amplified from *Botrytis* cDNA or plasmid DNA. Recipient vectors and fragments were cut using indicated restriction sites (Supplemental Table S3). Vectors were dephosphorylated prior to ligation and

fragment purified via gel extraction if necessary. For transient expression, pGreen II derivatives (pFF04 and pFF18) were used as recipient vectors (Künzl et al., 2016). Both vectors harbor a cauliflower mosaic virus (CMV) 35S promoter, an N-terminal SP and a kanamycin resistance cassette. A HA-tag for immunological detection was added at the C-terminus of the coding sequence via the reverse primers. For the generation of Hip1 lacking an SP (nospHip1), pFF18 was used without the N-terminal SP and a start codon was inserted before the Hip1 coding sequence. The Hip1-GFP fusion was constructed by GreenGate cloning (Lampropoulos et al., 2013), using the following modules: 35S promoter (pGGA004), ER signal sequence (pGGB006), linker-GFP (pGGD001) and RBCS terminator (pGGE001). The *hip1* coding sequence devoid of *Bsal* restriction sites for GreenGate cloning was synthesized by Biocat (Germany). For recombinant protein expression, the *hip1* sequence was amplified without SP and cloned into the pET28a (+) expression vector (Addgene, USA), eventually having a His-tag at the N-terminus. Sequences for cysteine point mutations were synthesized by Biocat (Germany) and cloned into pGreen II for transient expression. All primers used are shown in Supplemental Table S3. Gene constructs were verified by sequencing (Seq-It, Germany). For co-localization studies, the PM marker spRFP-TMD23 (pFK44) was used (Scheuring et al., 2012).

Secretome isolation and proteomics

Secretome samples were isolated from tomato leaves 48 h after *Botrytis* inoculation, as described previously (Müller et al., 2018).

Transient gene expression

A. tumefaciens (strain GV3101::mp90) was electroporated in the presence of 500 ng binary vector (pGreen II) using a gene pulser II (Bio-Rad, USA) set to 2.5 kV, 25 μF , and 400 Ω . For transient expression, overnight grown liquid cultures of transformed agrobacteria were washed with infiltration medium (Sparkes et al., 2006) and adjusted to the optical density (OD) 0.3 prior infiltrations in *N. benthamiana*. Subsequently, the infiltrated area was marked and assessed after 72 h incubation. The relative necrotic area was calculated as ratio of the infiltrated area and the necrotic area. For co-expression, agrobacteria cultures were adjusted to OD 0.15 and mixed before infiltration.

Protein extraction and immunological detection

Proteins were extracted from leaf disks (20 mm diameter) of infiltrated *N. benthamiana* by grinding in liquid nitrogen using a mortar and pestle. The frozen powder was suspended in extraction buffer (100 mM potassium, 20-mM 4-(2-hydroxyethyl)-1-piperazineethanesulfonic acid (HEPES), 0.1-mM ethylenediaminetetraacetic acid (EDTA), 2-mM DTT, 1-mM phenylmethylsulfonyl fluoride (PMSF); pH 7.5) and after centrifugation protein determination by Bradford was carried out. Equal protein amounts were separated via sodium dodecylsulfate polyacrylamide gel electrophoresis (SDS–

PAGE) and subsequently subjected to immunoblot on nitrocellulose membrane. Monoclonal antibodies against HA coupled to peroxidase (Roche; Cat. No. 12013819001, 1:1000 dilution) or GFP (Roche; 11814460001, 1:500 dilution) were used for chemiluminescence detection (ECL Prime Kit; Amersham, UK) on a FUSION detection system (Vilber Lourmat, FR).

RNA extraction and RT-qPCR

Total RNA of *Botrytis* infected or Hip1 infiltrated leaves was extracted using the NucleoSpin RNA Plant kit (Macherey-Nagel, Germany). RNA samples were reverse transcribed using the iScript cDNA synthesis kit (Bio-Rad, USA). RT-qPCR was performed with the PerfeCTa SYBR Green SuperMix (Quantabio, USA) in a CFX Connect Real-Time PCR Detection System (Bio-Rad, USA). Target-specific and control primers are listed in [Supplemental Table S3](#). Expression levels were normalized to the expression levels of Actin 2 (infections) or PP2A (infiltrations). Relative expression ratios were calculated according to the efficiency corrected calculation model (Pfaffl, 2001) or the $\Delta\Delta\text{CT}$ method when primers were described previously (Livak and Schmittgen, 2001).

Recombinant protein expression

Escherichia coli strains Rosetta pLysS (Novagen, USA) and T7 Shuffle (New England Biolabs, USA) were used to express Hip1. Protein expression was induced by 0.4 mM isopropyl β -D-1-thiogalactopyranoside (IPTG) and conducted at 37°C for 3 h or at 20°C overnight. After bacterial lysis, protein purification was carried out by immobilized metal affinity chromatography using His/Ni beads (Roth, Germany) as resin. Subsequently, dialysis was carried out using either 25 mM citrate buffer (pH 5) or 50 mM phosphate buffer with 150 mM NaCl (pH 6). For ethylene and ROS measurements, Hip1 protein was dialyzed against deionized H₂O.

Isolation of apoplastic fluid after transient expression

Seventy-two hours upon transformation, *N. benthamiana* leaves were incubated in 500 mL ddH₂O while a 60 mbar vacuum was applied for 10 min thrice. Next, the leaves were carefully placed in a syringe without a needle and centrifuged at 2,000g and 4°C for 15 min to collect the apoplastic fluid.

AlphaFold predictions

AlphaFold predictions were run on ColabFold (Mirdita et al., 2022) with a Colab Pro account and utilizing the AlphaFold2_advanced notebook (Jumper et al., 2021; Varadi et al., 2021). Search against genetic databases for MSA generation was done using mmseq2 with default options. AlphaFold was run in turbo mode to generate five prediction models. Each model contained one ensemble and one sample, and maximum number of recycles was set to 48. All five structures were refined with Amber-Relax yielding no observable effect on the protein structure. Prediction models

were ranked in confidence by the predicted local distance difference test (pLDDT) and the best-ranking model was selected for this article.

CD spectroscopy

Thermal un- and refolding were monitored between 15°C and 95°C at 215 nm with a Chirscan-plus spectrometer (Applied Photophysics, UK) equipped with a 150-W xenon arc lamp. The heating/cooling rate was 1°C min⁻¹. Samples contained about 15 μ M Hip1 and were measured using a 1 mm quartz glass cuvette (Hellma, Germany). Traces were normalized by assuming a completely folded state for the first 15 data points and a completely unfolded state for the last five data points. The mean of three experiments is shown in bold, individual measurements are displayed in light blue/red.

Confocal microscopy

Images were acquired using a Zeiss LSM880 AxioObserver confocal laser scanning microscope equipped with a Zeiss C-Apochromat 40 \times /1.2 W AutoCorr M27 water-immersion objective (INST 248/254-1). Fluorescent signals of GFP (excitation/emission 488 nm/500–571 nm) and red fluorescent protein (RFP) (excitation/emission 543 nm/580–718 nm) were processed using the Zeiss software ZEN 2.3 or ImageJ (<https://imagej.nih.gov/ij/>). Laser intensity was set to 2% and the gains were adjusted in accordance with the protein expression level. For co-expression studies, images were acquired using sequential scan mode to avoid channel cross-talk.

ROS assays

ROS production was measured as described by (Ranf et al., 2015). Small leaf discs (3-mm diameter) of *N. benthamiana* plants were cut and floated overnight on 200 μ L ddH₂O in a 96-well plate (one disc per well; white 96-well plates). Before starting the measurement, the water was removed with a pipette and 75 μ L of Luminol-Mastermix (2 μ g mL⁻¹ horseradish peroxidase (Type II, Roche), 5 μ M L-012; WAKO chemicals) was added into each well. Luminescence was measured as relative light units (RLU) in 1-min interval using a Tecan F200 luminometer. The background was measured for 10 min. The elicitors were always added in a volume of 25 μ L diluted with Luminol-Mastermix. After elicitor treatment luminescence readings were continued for 90 min. Data are shown after normalization to average ROS levels 5 min before elicitor application and subtraction of water controls that were included for each genotype on the same plate.

Ethylene measurements

Nicotiana benthamiana leaf discs (3 mm) floated overnight on ddH₂O. Three leaf discs were put into one glass vial (6 mL volume) with 200 μ L ddH₂O. The respective elicitor or ddH₂O as control was added and the vials were closed with a rubber cap. The samples were shaken for 3 h at 100 rpm on a horizontal shaker. One milliliter air was taken out

through the rubber cap with a syringe and injected into a gas chromatograph. Each treatment was measured with three replicates.

Determination of phytohormones via ultra performance liquid chromatography (UPLC)-MS/MS

Phytohormone content was analyzed as described by Salem et al. (2020). In brief, 40–50 mg frozen plant material was extracted with 750 μL methyl tert-butyl ether (MTBE) for 30 min at 4°C at 1,000 rpm, followed by incubation for 15 min in an ultrasonic ice bath. Samples were centrifuged for 10 min at 4°C and 10,000g. Supernatants were transferred into new reaction tubes. An equal volume of 0.1% (v/v) HCl in water was added to the MTBE extract and incubated for another 30 min at 4°C at 1,000 rpm. After 10 min centrifugation at 4°C and 10,000g, the upper phase (green color) was transferred to a new 1.5-mL reaction tube and dried in a vacuum concentration system (SpeedVac, Eppendorf) at RT. Immediately before analysis, dried samples were reconstituted in 50 μL 50% (v/v) methanol (in water) by vortexing for 3 min. Chromatographic conditions and mass spectrometry parameters were used as described (Salem et al., 2020).

Calcein release assay

Calcein-filled PM vesicles were prepared from six-week-old *N. benthamiana* as described (Ottmann et al., 2009). Permeabilization of the vesicles (1 ng protein μL^{-1}) induced by Hip1 or *P. parasitica* NLP (expressed as described; Ottmann et al., 2009) was assayed at RT in 20 mM 2-(N-morpholino)ethanesulfonic acid (MES), pH 5.8, 140-mM NaCl by measuring fluorescence (excitation 485 ± 14 nm, emission 535 ± 20 nm) in a microplate reader (TriStar 5, Berthold). The percentage of calcein release (R) was calculated according to the equation

$$R = (F_{\text{meas}} - F_{\text{init}}) / (F_{\text{max}} - F_{\text{init}}) * 100,$$

where F_{meas} , F_{init} , and F_{max} are the measured, initial, and maximal fluorescence, respectively. F_{max} was obtained by the addition of Triton X-100 to 0.5% (v/v) final concentration at the end of each measurement.

Virus-induced gene silencing

Silencing of *SOBIR1* and *BAK1* in *N. benthamiana* plants was performed using the tobacco rattle virus (TRV)-based plasmid construct pTRV2 with *A. tumefaciens* (strain GV3101::mp90), as described previously in (Seifbarghi et al., 2020). Twenty days later, attached leaves were infiltrated with 15 μM Hip1 protein, and necrosis development was quantified after 48 h.

CRISPR/Cas9-mediated generation of *Botrytis* overexpressor strains

Synthesis of single guide RNA and ribonucleoprotein complexes (RNP) formation has been carried out as described previously (Leisen et al., 2020). To overexpress Hip1, a construct harboring Hip1 under the control of the *Botrytis* H2B

promoter plus a hygromycin cassette was generated. The recipient vector pBS_Hyg was generated as follows: a hygromycin cassette under the control of PtrpC was amplified from pNAH-OGG (Schumacher et al., 2013) using the primers PtrpC_KpnI_FW and Hyg_Sall_RV (Supplementary Table S3). The Tniad terminator was amplified from pTEL-Fen (Leisen et al., 2020) using Tniad_Sall_FW and Tniad_XbaI_RV. Fragments were prepared using the indicated restriction sites and ligated into the vector pBS KS. *hip1* was amplified using Hip1_SalI_FW and Hip_SacI_RV and the H2B promoter from genomic DNA by using H2B_NotI_FW and H2B_RV. Fragments were prepared using the indicated restriction sites and ligated into pBS_Hyg generating the pBS-Hyg-Hip1 overexpression construct. For genomic integration, a fragment harboring the hygromycin cassette and *hip1* driven by the H2B promoter was amplified using M13FW_left_60bp and M13RV_right_60bp. DNA double-strand break was induced by CRISPR/Cas9 and a sgRNA based on the protospacer-specific oligonucleotides sgRNA (Supplementary Table S3). Transformation of *Botrytis* was performed as described previously (Leisen et al., 2020).

Microscopy analysis of infection

To compare early infection and colonization of *Botrytis* wild type and *hip1* overexpression strains, inoculations of detached *P. vulgaris* leaves were performed and microscopically analyzed. Leaves were inoculated with 1 μL of 10^5 conidia mL^{-1} in GB5 medium with 25-mM glucose. After 20 h, developing lesions were stained with 10 $\mu\text{g mL}^{-1}$ calcofluor white (fluorescence brightener 28, Sigma) for 5 min and thoroughly washed with water subsequently. Calcofluor white was excited with 405 nm, and emission was detected with 416–519 nm and chlorophyll autofluorescence with 633 nm and 638–721 nm, respectively.

Statistical analysis

Analysis was carried out using the GraphPad Prism 9 software. The detailed statistical method employed is provided in the respective figure legends. All experiments were carried out at least three times. Box limits in the graphs represent 25th to 75th percentile, the horizontal line the median and whiskers minimum to maximum values.

Accession numbers

Sequence data from this article can be found in the GenBank/EMBL data libraries under the accession numbers provided in Supplementary Table S1.

Supplemental data

The following materials are available in the online version of this article.

Supplemental Figure S1. Toxicity of secreted proteins and other compounds from *Botrytis* rely on protein activity.

Supplemental Figure S2. Transient expression control of candidates from *Botrytis*.

Supplemental Figure S3. Expression control of truncated Hip1 derivatives and cysteine mutants.

Supplemental Figure S4. Protein expression and structure prediction of Hip1.

Supplemental Figure S5. Hip1 toxicity is unaltered when fused to GFP but dependence on the presence of a SP.

Supplemental Figure S6. Virus-induced gene silencing of BAK1 and SOBIR1 in *N. benthamiana*.

Supplemental Figure S7. Analysis of *Botrytis hip1* overexpression strains.

Supplemental Figure S8. Secondary lesion formation by *Botrytis*.

Supplemental Table S1. List of tested candidate genes.

Supplemental Table S2. Alignment of Hip1 homologs.

Supplemental Table S3. Primers used in this study.

Acknowledgments

We would like to thank Peter Pimpl for providing the vectors pFF04 and pFF18 and Matthieu Joosten for the SOBIR1/SOBIR1-like *N. benthamiana* knockout lines. For the alpha-fold prediction we thank Jonas Höring. Furthermore, technical help from Oliver Trentmann, Sarah Gabelmann, Tabea Lang, Patrick Pattar, Marco Aras, and Benjamin Ledermann is highly appreciated. For the kind willingness to share facilities and equipment, we thank Michael Schroda and Nicole Frankenberg-Dinkel. We thank the Metabolomics Core Technology Platform of Heidelberg University for support with UPLC-MS/MS-based phytohormone quantification.

Funding

This work was supported by grants from the *BioComp* research initiative (Rhineland-Palatinate, Germany), the TU-Nachwuchsring (University of Kaiserslautern) and the German research foundation (DFG; SCHE 1836/4-1 and SCHE 1836/5-1) to D.S.

Conflict of interest statement. None declared.

References

- Albert I, Böhm H, Albert M, Feiler CE, Imkampe J, Wallmeroth N, Brancato C, Raaymakers TM, Oome S, Zhang H, et al. (2015) An RLP23-SOBIR1-BAK1 complex mediates NLP-triggered immunity. *Nat Plants* **1**: 15140
- Boutrot F, Zipfel C (2017) Function, discovery, and exploitation of plant pattern recognition receptors for broad-spectrum disease resistance. *Ann Rev Phytopathol* **55**: 257–286
- Brito N, Espino JJ, González C (2006) The endo-beta-1,4-xylanase xyn11A is required for virulence in *Botrytis cinerea*. *Mol Plant Microbe Interact* **19**: 25–32
- Chruszcz M, Chapman MD, Osinski T, Solberg R, Demas M, Porebski PJ, Majorek KA, Pomés A, Minor W (2012) *Alternaria alternata* allergen Alt a 1: a unique β -barrel protein dimer found exclusively in fungi. *J Allergy Clin Immunol* **130**: 241–7.e9
- Cuesta Arenas Y, Kalkman ERIC, Schouten A, Dieho M, Vredenburg P, Uwumukiza B, Osés Ruiz M, van Kan JAL (2010) Functional analysis and mode of action of phytotoxic Nep1-like proteins of *Botrytis cinerea*. *Physiol Mol Plant Pathol* **74**: 376–386
- Dean R, van Kan JAL, Pretorius ZA, Hammond-Kosack KE, Di Pietro A, Spanu PD, Rudd JJ, Dickman M, Kahmann R, Ellis J, et al. (2012) The top 10 fungal pathogens in molecular plant pathology. *Mol Plant Pathol* **13**: 804
- Engelhardt S, Lee J, Gäbler Y, Kemmerling B, Haapalainen M-L, Li C-M, Wei Z, Keller H, Joosten M, Taira S, et al. (2009) Separable roles of the *Pseudomonas syringae* pv. phaseolicola accessory protein HrpZ1 in ion-conducting pore formation and activation of plant immunity. *Plant J* **57**: 706–717
- Espino JJ, Brito N, Noda J, González C (2005) *Botrytis cinerea* endo- β -1,4-glucanase Cel5A is expressed during infection but is not required for pathogenesis. *Physiol Mol Plant Pathol* **66**: 213–221
- Espino JJ, Gutiérrez-Sánchez G, Brito N, Shah P, Orlando R, González C (2010) The *Botrytis cinerea* early secretome. *Proteomics* **10**: 3020–3034
- Fan L, Fröhlich K, Melzer E, Pruitt RN, Albert I, Zhang L, Joe A, Hua C, Song Y, Albert M et al. (2022) Genotyping-by-sequencing-based identification of Arabidopsis pattern recognition receptor RLP32 recognizing proteobacterial translation initiation factor IF1. *Nat Commun* **13**: 1294
- Felix G, Duran JD, Volko S, Boller T (1999) Plants have a sensitive perception system for the most conserved domain of bacterial flagellin. *Plant J Cell Mol Biol* **18**: 265–276
- Friás M, Brito N, González M, González C (2014) The phytotoxic activity of the cerato-platanin BcSpl1 resides in a two-peptide motif on the protein surface. *Mol Plant Pathol* **15**: 342–351
- Friás M, González C, Brito N (2011) BcSpl1, a cerato-platanin family protein, contributes to *Botrytis cinerea* virulence and elicits the hypersensitive response in the host. *New Phytol* **192**: 483–495
- Friás M, González M, González C, Brito N (2016) BcIEB1, a *Botrytis cinerea* secreted protein, elicits a defense response in plants. *Plant Sci* **250**: 115–124
- Gaulin E, Jauneau A, Villalba F, Rickauer M, Esquerré-Tugayé M-T, Bottin A (2002) The CBEL glycoprotein of *Phytophthora parasitica* var. *nicotianae* is involved in cell wall deposition and adhesion to cellulosic substrates. *J Cell Sci* **115**: 4565–4575
- Govrin EM, Levine A (2000) The hypersensitive response facilitates plant infection by the necrotrophic pathogen *Botrytis cinerea*. *Current Biol* **10**: 751–757
- Govrin EM, Rachmilevitch S, Tiwari BS, Solomon M, Levine A (2006) An Elicitor from *Botrytis cinerea* induces the hypersensitive response in *Arabidopsis thaliana* and other plants and promotes the gray mold disease. *Phytopathol* **96**: 299–307
- He SY, Huang H-C, Collmer A (1993) *Pseudomonas syringae* pv. *syringae* harpinPss: A protein that is secreted via the hrp pathway and elicits the hypersensitive response in plants. *Cell* **73**: 1255–1266
- Hématy K, Cherk C, Somerville S (2009) Host-pathogen warfare at the plant cell wall. *Curr Opin Plant Biol* **12**: 406–413
- Huang WRH, Schol C, Villanueva SL, Heidstra R, Joosten MHAJ (2021) Knocking out SOBIR1 in *Nicotiana benthamiana* abolishes functionality of transgenic receptor-like protein Cf-4. *Plant Physiol* **185**: 290–294
- Jones JDG, Dangl JL (2006) The plant immune system. *Nature* **444**: 323–329
- Jumper J, Evans R, Pritzel A, Green T, Figurnov M, Ronneberger O, Tunyasuvunakool K, Bates R, Židek A, Potapenko A, et al. (2021) Highly accurate protein structure prediction with AlphaFold. *Nature* **596**: 583–589
- Kars I, Krooshof GH, Wagemakers L, Joosten R, Benen JAE, van Kan JAL (2005) Necrotizing activity of five *Botrytis cinerea* endopolygalacturonases produced in *Pichia pastoris*. *Plant J* **43**: 213–225
- Kelley LA, Mezulis S, Yates CM, Wass MN, Sternberg MJE (2015) The Phyre2 web portal for protein modeling, prediction and analysis. *Nature Protoc* **10**: 845–858
- Kettles GJ, Bayon C, Canning G, Rudd JJ, Kanyuka K (2017) Apoplastic recognition of multiple candidate effectors from the wheat pathogen *Zymoseptoria tritici* in the nonhost plant *Nicotiana benthamiana*. *New Phytol* **213**: 338–350

- Khatib M, Lafitte C, Esquerre-Tugay M-T, Bottin A, Rickauer M** (2004) The CBEL elicitor of *Phytophthora parasitica* var. *nicotianae* activates defence in *Arabidopsis thaliana* via three different signalling pathways. *New Phytol* **162**: 501–510
- Künzl F, Frühholz S, Fäßler F, Li B, Pimpl P** (2016) Receptor-mediated sorting of soluble vacuolar proteins ends at the trans-Golgi network/early endosome. *Nat Plants* **2**: 16017
- Lampropoulos A, Sutikovic Z, Wenzl C, Maegele I, Lohmann JU, Forner J** (2013) GreenGate—A novel, versatile, and efficient cloning system for plant transgenesis. *PLoS ONE* **8**: e83043
- Leisen T, Bietz F, Werner J, Wegner A, Schaffrath U, Scheuring D, Willmund F, Mosbach A, Scalliet G, Hahn M** (2020) CRISPR/Cas with ribonucleoprotein complexes and transiently selected telomere vectors allows highly efficient marker-free and multiple genome editing in *Botrytis cinerea*. *PLoS Pathog* **16**: e1008326
- Leisen T, Werner J, Pattar P, Safari N, Ymeri E, Sommer F, Schroada M, Suarez I, Collado IG, Scheuring D** (2022) Multiple knockout mutants reveal a high redundancy of phytotoxic compounds contributing to necrotrophic pathogenesis of *Botrytis cinerea*. *PLoS Pathog* **18**: e1010367
- Lenarčić T, Albert I, Böhm H, Hodnik V, Pirc K, Zavec AB, Podobnik M, Pahovnik D, Žagar E, Pruitt R** (2017) Eudicot plant-specific sphingolipids determine host selectivity of microbial NLP cytolytins. *Science* **358**: 1431–1434
- Li B, Wang W, Zong Y, Qin G, Tian S** (2012) Exploring pathogenic mechanisms of *Botrytis cinerea* secretome under different ambient pH based on comparative proteomic analysis. *J Proteome Res* **11**: 4249–4260
- Livak KJ, Schmittgen TD** (2001) Analysis of relative gene expression data using real-time quantitative PCR and the $2^{-\Delta\Delta C_T}$ Method. *Methods* **25**: 402–408
- Mengiste T** (2012) Plant immunity to necrotrophs. *Ann Rev Phytopathol* **50**: 267–294
- Mirdita M, Schütze K, Moriwaki Y, Heo L, Ovchinnikov S, Steinegger M** (2022) ColabFold: Making protein folding accessible to all. *Nat Methods* **19**: 679–682
- Müller N, Leroch M, Schumacher J, Zimmer D, Könnel A, Klug K, Leisen T, Scheuring D, Sommer F, Mühlhaus T, et al.** (2018) Investigations on VELVET regulatory mutants confirm the role of host tissue acidification and secretion of proteins in the pathogenesis of *Botrytis cinerea*. *New Phytol* **219**: 1062–1074
- Nie J, Yin Z, Li Z, Wu Y, Huang L** (2019) A small cysteine-rich protein from two kingdoms of microbes is recognized as a novel pathogen-associated molecular pattern. *New Phytol* **222**: 995–1011
- Nie J, Zhou W, Liu J, Tan N, Zhou J-M, Huang L** (2020) A receptor-like protein from *Nicotiana benthamiana* mediates VmE02 PAMP-triggered immunity. *New Phytol* **229**: 2260–2272
- Noda J, Brito N, González C** (2010) The *Botrytis cinerea* xylanase Xyn11A contributes to virulence with its necrotizing activity, not with its catalytic activity. *BMC plant biology* **10**: 38
- Oliver RP, Solomon PS** (2010) New developments in pathogenicity and virulence of necrotrophs. *Curr Opin Plant Biol* **13**: 415–419
- Ottmann C, Luberacki B, Küfner I, Koch W, Brunner F, Weyand M, Mattinen L, Pirhonen M, Anderluh G, Seitz HU, et al.** (2009) A common toxin fold mediates microbial attack and plant defense. *Proc Natl Acad Sci USA* **106**: 10359–10364
- Pfaffl MW** (2001) A new mathematical model for relative quantification in real-time RT-PCR. *Nucleic Acids Res* **29**: e45
- Pitsili E, Phukan UJ, Coll NS** (2020) Cell death in plant immunity. *Cold Spring Harb Perspect Biol* **12**: a036483
- Ranf S, Gisch N, Schäffer M, Illig T, Westphal L, Knirel YA, Sánchez-Carballo PM, Zähringer U, Hückelhoven R, Lee J, et al.** (2015) A lectin S-domain receptor kinase mediates lipopolysaccharide sensing in *Arabidopsis thaliana*. *Nat Immunol* **16**: 426–433
- Salem MA, Yoshida T, Perez de Souza L, Alseikh S, Bajdzienko K, Fernie AR, Giavalisco P** (2020) An improved extraction method enables the comprehensive analysis of lipids, proteins, metabolites and phytohormones from a single sample of leaf tissue under water-deficit stress. *Plant J* **103**: 1614–1632
- Schellenberger R, Touchard M, Clément C, Baillieux F, Cordelier S, Crouzet J, Dorey S** (2019) Apoplastic invasion patterns triggering plant immunity: plasma membrane sensing at the frontline. *Mol Plant Pathol* **20**: 1602–1616
- Scheuring D, Künzl F, Viotti C, Yan MSW, Jiang L, Schellmann S, Robinson DG, Pimpl P** (2012) Ubiquitin initiates sorting of Golgi and plasma membrane proteins into the vacuolar degradation pathway. *BMC Plant Biol* **12**: 164
- Schouten A, van Baarlen P, van Kan JAL** (2008) Phytotoxic Nep1-like proteins from the necrotrophic fungus *Botrytis cinerea* associate with membranes and the nucleus of plant cells. *New Phytol* **177**: 493–505
- Schumacher J, Gautier A, Morgant G, Studt L, Ducrot P-H, Le Pêcheur P, Azeddine S, Fillinger S, Leroux P, Tudzynski B, et al.** (2013) A functional bikaverin biosynthesis gene cluster in rare strains of *Botrytis cinerea* is positively controlled by VELVET. *PLOS ONE* **8**: e53729
- Seifbarghi S, Borhan MH, Wei Y, Ma L, Coutu C, Bekkaoui D, Hegedus DD** (2020) Receptor-like kinases BAK1 and SOBIR1 are required for necrotizing activity of a novel group of sclerotinia sclerotiorum necrosis-inducing effectors. *Frontier Plant Sci* **11**: 1021
- Sparkes IA, Runions J, Kearns A, Hawes C** (2006) Rapid, transient expression of fluorescent fusion proteins in tobacco plants and generation of stably transformed plants. *Nature Protoc* **1**: 2019–2025
- Taylor RD, Saparno A, Blackwell B, Anoop V, Gleddie S, Tinker NA, Harris LJ** (2008) Proteomic analyses of *Fusarium graminearum* grown under mycotoxin-inducing conditions. *Proteomics* **8**: 2256–2265
- Ten Have A, Mulder W, Visser J, van Kan JA** (1998) The endopolygalacturonase gene *Bcpg1* is required for full virulence of *Botrytis cinerea*. *Molecular plant-microbe interactions: MPMI* **11**: 1009–1016
- Thomma BPHJ, Nürnberger T, Joosten MHAJ** (2011) Of PAMPs and effectors: The blurred PTI-ETI dichotomy. *Plant Cell* **23**: 4–15
- van Kan JAL** (2006) Licensed to kill: The lifestyle of a necrotrophic plant pathogen. *Trends Plant Sci* **11**: 247–253
- van Kan JA, van't Klooster JW, Wagemakers CA, Dees DC, van der Vlugt-Bergmans CJ** (1997) Cutinase A of *Botrytis cinerea* is expressed, but not essential, during penetration of gerbera and tomato. *Mol Plant Microbe Interact* **10**: 30–38
- Varadi M, Anyango S, Deshpande M, Nair S, Natassia C, Yordanova G, Yuan D, Stroe O, Wood G, Laydon A et al.** (2021) AlphaFold protein structure database: Massively expanding the structural coverage of protein-sequence space with high-accuracy models. *Nucleic Acids Res* **50**: D439–D444
- Veloso J, van Kan JAL** (2018) Many shades of grey in *Botrytis*-Host plant interactions. *Trends Plant Sci* **23**: 613–622
- Veronese P, Chen X, Bluhm B, Salmeron J, Dietrich R, Mengiste T** (2004) The BOS loci of *Arabidopsis* are required for resistance to *Botrytis cinerea* infection. *Plant J* **40**: 558–574
- Wang B, Yang X, Zeng H, Liu H, Zhou T, Tan B, Yuan J, Guo L, Qiu D** (2012) The purification and characterization of a novel hypersensitive-like response-inducing elicitor from *Verticillium dahliae* that induces resistance responses in tobacco. *Appl Microbiol Biotechnol* **93**: 191–201
- Weiberg A, Wang M, Lin F-M, Zhao H, Zhang Z, Kaloshian I, Huang H-D, Jin H** (2013) Fungal small RNAs suppress plant immunity by hijacking host RNA interference pathways. *Science* **342**: 118–123
- Williamson B, Tudzynski B, Tudzynski P, van Kan JAL** (2007) *Botrytis cinerea*: the cause of grey mould disease. *Mol Plant Pathol* **8**: 561–580
- Yang D, Jeng RS, Hubbes M** (1989) Mansonone accumulation in elm callus induced by elicitors of *Ophiostoma ulmi*, and general properties of elicitors. *Can J Bot* **67**: 3490–3497

- Yang Y, Yang X, Dong Y, Qiu D** (2018) The *Botrytis cinerea* Xylanase BcXyl1 modulates plant immunity. *Frontiers in Microbiology* **9**: 2535
- Zhang Y, Gao Y, Liang Y, Dong Y, Yang X, Qiu D** (2019) *Verticillium dahliae* PevD1, an Alt a 1-like protein, targets cotton PR5-like protein and promotes fungal infection. *J Exp Bot* **70**: 613–626
- Zhang L, Hua C, Pruitt RN, Qin S, Wang L, Albert I, Albert M, van Kan JAL, Nürnberger T** (2021) Distinct immune sensor systems for fungal endopolygalacturonases in closely related Brassicaceae. *Nat Plants* **7**: 1254–1263
- Zhang L, Kars I, Essenstam B, Liebrand TWH, Wagemakers L, Elberse J, Tagkalaki P, Tjoitang D, van den Ackerveken G, van Kan JAL** (2014b) Fungal endopolygalacturonases are recognized as microbe-associated molecular patterns by the arabidopsis receptor-like protein responsiveness to *Botrytis polygalacturonases*1. *Plant Physiology* **164**: 352–364
- Zhang Y, Liang Y, Dong Y, Gao Y, Yang X, Yuan J, Qiu D** (2017) The *Magnaporthe oryzae* Alt A 1-like protein MoHrip1 binds to the plant plasma membrane. *Biochem Biophys Res Commun* **492**: 55–60
- Zhang H, Wu Q, Cao S, Zhao T, Chen L, Zhuang P, Zhou X, Gao Z** (2014a) A novel protein elicitor (SsCut) from *Sclerotinia sclerotiorum* induces multiple defense responses in plants. *Plant Mol Biol* **86**: 495–511
- Zhou R, Zhu T, Han L, Liu M, Xu M, Liu Y, Han D, Qiu D, Gong Q, Liu X** (2017) The asparagine-rich protein NRP interacts with the *Verticillium* effector PevD1 and regulates the subcellular localization of cryptochrome 2. *J Exp Botany* **68**: 3427–3440
- Zhu W, Ronen M, Gur Y, Minz-Dub A, Masrati G, Ben-Tal N, Savidor A, Sharon I, Eizner E, Valerius O, et al.** (2017) BcXYG1, a Secreted Xyloglucanase from *Botrytis cinerea*, triggers both cell death and plant immune responses1. *Plant Physiol* **175**: 438–456